AIP | Review of Scientific Instruments

Influence of ion source configuration and its operation parameters on the target sputtering and implantation process

K. V. Shalnov, V. R. Kukhta, K. Uemura, and Y. Ito

Citation: Rev. Sci. Instrum. **83**, 063304 (2012); doi: 10.1063/1.4731009
View online: http://dx.doi.org/10.1063/1.4731009
View Table of Contents: http://rsi.aip.org/resource/1/RSINAK/v83/i6
Published by the American Institute of Physics.

Influence of ion source configuration and its operation parameters on the target sputtering and implantation process

K. V. Shalnov,[1,a)] V. R. Kukhta,[1] K. Uemura,[1] and Y. Ito[2]
[1]*Nagata Seiki Co, 8-2, Kamisuwa, Tsubame-shi, Niigata-ken, 959-0181, Japan*
[2]*Nagaoka University of Technology, Nagaoka, 940-2188, Japan*

(Received 29 March 2012; accepted 10 June 2012; published online 27 June 2012)

In the work, investigation of the features and operation regimes of sputter enhanced ion-plasma source are presented. The source is based on the target sputtering with the dense plasma formed in the crossed electric and magnetic fields. It allows operation with noble or reactive gases at low pressure discharge regimes, and, the resulting ion beam is the mixture of ions from the working gas and sputtering target. Any conductive material, such as metals, alloys, or compounds, can be used as the sputtering target. Effectiveness of target sputtering process with the plasma was investigated dependently on the gun geometry, plasma parameters, and the target bias voltage. With the applied accelerating voltage from 0 to 20 kV, the source can be operated in regimes of thin film deposition, ion-beam mixing, and ion implantation. Multi-component ion beam implantation was applied to α-Fe, which leads to the surface hardness increasing from 2 GPa in the initial condition up to 3.5 GPa in case of combined N_2-C implantation. Projected range of the implanted elements is up to 20 nm with the implantation energy 20 keV that was obtained with XPS depth profiling. © *2012 American Institute of Physics*. [http://dx.doi.org/10.1063/1.4731009]

I. INTRODUCTION

Multi-component or mixed ion beams attract considerable interests for the industrial applications. They can be utilized for such tasks as: (1) surface layers physical or chemical properties modification with ion implantation technique; (2) ion-beam assisted deposition (IBAD) of multi-component layers; (3) ion-beam mixing for nanostructures or interlayers formation and other. Application of multi-component beams can provide significant advantage for the materials treatment process both from technological and from economic points of view. In the case of ion implantation, there are much of examples of multi-component implantation (gas and metal ions) being more effective comparing to a single component one;[1,2] it is also known that IBAD is the effective technique for the dense thin films deposition, having much of advantage over the conventional deposition techniques for the process and coating properties control.[3,4] Usually, for the tasks of multi-component beams treatment, subsequent treatments with two or more ion species are applied, or, the combined systems where two or more ions or atoms sources are utilized for simultaneous treatment.[5,6] Industrial application of those systems should be rather expensive and complex for the operation and control.

One of the promising types of the ion sources, which can meet with the technological and economic requirements of the industrial applications, is the devices with cathodic sputtering. In the devices, gas plasma is applied for the sputtering of target electrode and, with following ionization of the sputtered particles, the multi-component plasma can be obtained. Resulting plasma consists with ions from the working gas and with ions from the sputtering target. The target can be made with any conductive material: metals, alloys, or compound. Previously, it was demonstrated by Potemkin *et al.*[7] that ion sources, based on such principle, utilizing low pressure discharge plasma in crossed electric and magnetic fields, and, with optimal configuration of the electrodes can be an effective tool for the generation of multi-component plasma, and, it can produce intense non-separated beams of gas and metal ions. In the devices, there are neither droplet phase nor multicharged ions usually. For the technological tasks, connected with the ion implantation or ion beam mixing, possibilities to apply the devices were demonstrated as well.[8,9]

In spite of principal simplicity, there are certain difficulties with the design and operation of the devices with the cathodic sputtering. Due to the complex multistep nature of the plasma formation process, all components of the source must be matched to each other for effective and reliable operation. Concentration of the sputtered particles in the plasma, which is determined by the target sputtering efficiency, depends on the plasma properties and electrodes system configuration. So far, it can be said that the issues of construction influence and operation parameters on the target sputtering process were not well investigated and followed to further study.

In the work, the brief description of the experimental setup is presented. The setup is equipped with the constructed sputter enhanced ion-plasma source. The source principle is based on the preceding investigations.[7,9] Previously, the setup, with TiB_2 sputtering target, was applied for the surface properties modification of construction steels and alloys, as well as for the commercial products, such as cutting tools and metal dies.[10] Here, the investigation of the ion-plasma source parameters was performed from the point of view of the effectiveness of target sputtering. Influences of electrodes geometry, ion current density, sputtering, and acceleration voltages

a)Author to whom correspondence should be addressed. Electronic mail: konstantin_shaln@itac-j.co.jp.

were investigated. Thickness and composition of deposited layers were evaluated as the measure of target sputtering effectiveness. With the acceleration voltage from 0 to 20 kV, the effect of multi-component ion beam on the surface layer was investigated dependently from effectiveness of target sputtering. Examples of mixed beam ion implantations are presented and discussed.

II. EXPERIMENTAL SETUP

In Fig. 1, photos of the constructed sputter enhanced ion-plasma source (a) and outlook of source exit aperture (b) are presented. Schematic diagram of the experimental setup is presented in Fig. 2. The ion-plasma source is installed on the top flange of the vacuum chamber (Fig. 2(9)). The vacuum chamber has cylindrical shape with height ~770 mm and internal diameter ~900 mm. Vacuum system consisting with the mechanical and diffusion pumps provides the initial pressure in the vacuum chamber $\sim 2\times10^{-4}$ Pa and the typical working pressure is $\sim$1-2$\times10^{-2}$ Pa. Round shape high-voltage accelerating electrode (Fig. 2(8)) with diameter ~250 mm, which acts as a samples holder, is installed coaxial to the source axis on the vacuum chamber bottom flange through the insulator.

Detail explanation of the operation principle of the reported kind of ion-plasma sources can be found in Ref. 9 for an example. Here, selective points, important for our investigations, are described.

The source has axial symmetric geometry. Firstly, with the low pressure discharge, plasma is initiated in the crossed electric and magnetic field in the ring-shape chamber between water-cooled ring-shape anode (Fig. 2(3)) and circular discharge cathodes (Fig. 2(4)). Cathodes have blade-shape edges for the efficient discharge ignition, which is obtained due to the field concentration near the blade edges and due to the efficient field electron emission. Magnetic system, which is formed with two permanent ring magnets (Fig. 2(2)), magnetically conductive source body (Fig. 2(1)) and discharge cathodes (Fig. 2(4)), creates non-uniform magnetic field in the discharge region and allows non-uniform plasma to be obtained with the maximal density near the discharge slit formed by the top and bottom cathodes. Plasma density of the low pressure discharge in the discharge region can be up to 10^{11} cm^{-3} and the electron temperature up to 10 eV.[9]

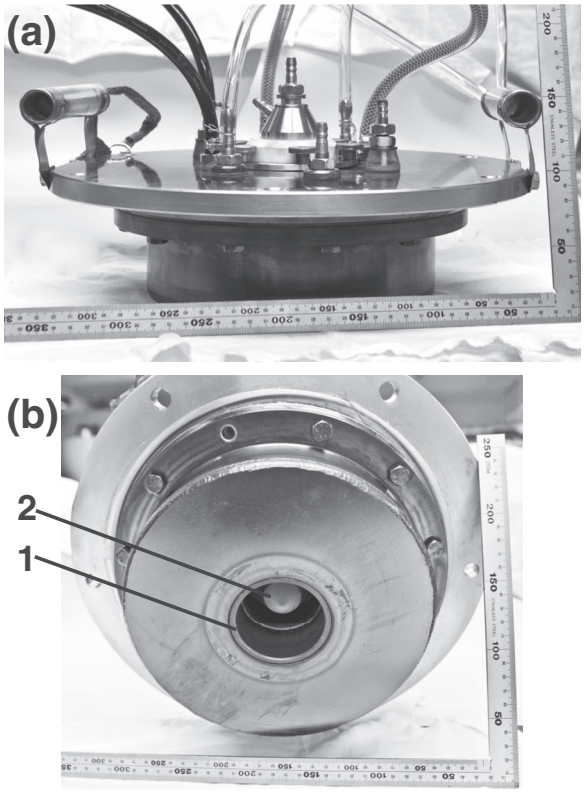

FIG. 1. (a) Photo of sputter enhanced ion-plasma source; (b) bottom source view with 1 – exit aperture (diam. – 60 mm), 2 – sputtering target.

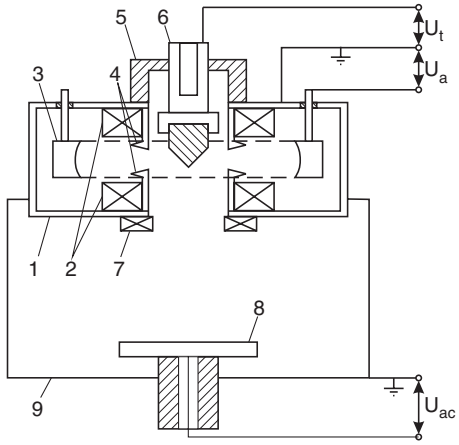

FIG. 2. Schema of the experimental setup equipped with the sputter enhanced ion-plasma source. 1 – water-cooled source body; 2 – permanent ring-shape magnets, 3 – water-cooled ring-shape anode; 4 – top and bottom discharge cathodes; 5 – ceramic insulator; 6 – sputtering target unit; 7 – plasma stabilizing permanent magnet; 8 – accelerating electrode; 9 – vacuum chamber; U_a – plasma discharge voltage; U_t – sputtering target bias voltage; U_{ac} – accelerating voltage.

Due to the plasma sputtering of the walls of discharge chamber and cathodes, some ingress of walls and cathodes material to the plasma can be anticipated. Shape of the discharge cathodes (Fig. 2(4)) was optimized to reduce the plasma contamination with the wall material (steel) as well as taking into account the discharge stability and ignition facilitation.

Dependently on gas pressure, with the obtained configurations of electric and magnetic fields, plasma can be sustained in two regimes: (1) "low voltage – high current" regime with ignition voltage $U_a < 500$ V and plasma current $I_a \sim 0.6$ – 2 A. The regime, initiated at working pressures $P \geq 0.013$ Pa, is characterized with the stable discharge burning in the discharge region with maximum density near the cathodes slit and can be described as typical glow discharge in the crossed fields. For example, Fig. 3 exhibits the current – voltage characteristics of plasma for argon and nitrogen gases at higher and lower pressures as for the "low voltage – high current" plasma burning regime. It can be observed that dependence is linear and higher pressure gives lower discharge burning voltage. (2) "High voltage – low current" regime which is initiated at the pressures $P < 0.011$ Pa with the ignition voltage $U_a > 1000$ V and plasma current $I_a < 0.1$ A. Plasma density, in the case, is low and the regime is not considered for visible operation, but, on the other hand, it can be utilized for

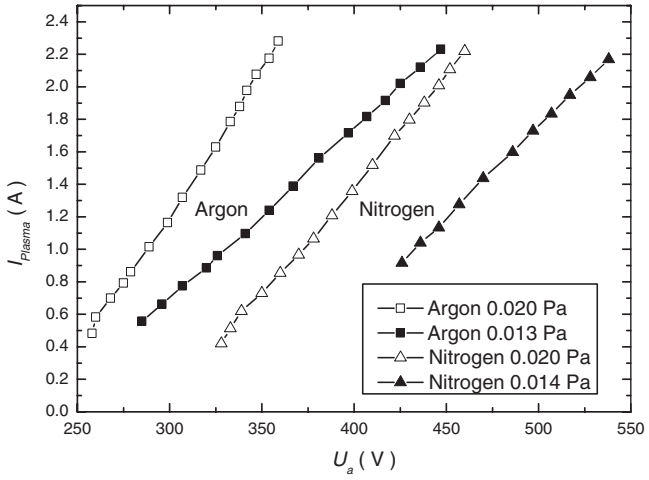

FIG. 3. Typical current-voltage characteristics of low pressure plasma in the source discharge chamber for argon and nitrogen gases at different working pressures.

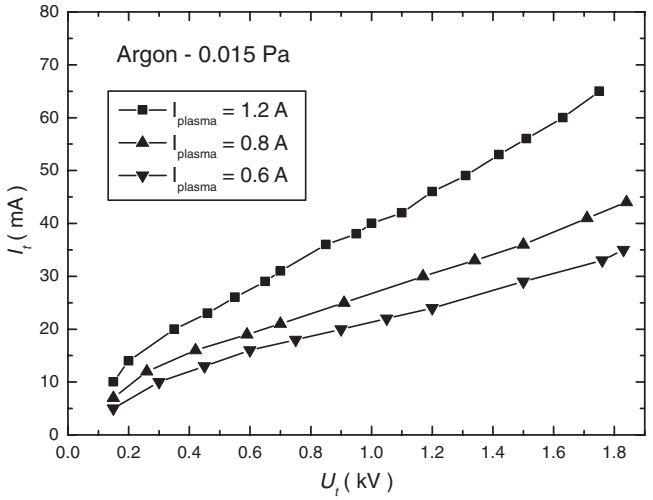

FIG. 4. Titanium target ion current I_t as a function of sputtering voltage U_t for the different plasma currents at working pressure of Ar gas 0.015 Pa.

the plain gas ion implantation with the low ion current. Also, in the pressure range $0.010 < P < 0.013$ Pa, plasma acts in the transition regime with the pulsations in the central source chamber near the exit aperture. This regime is less stable and difficult to control.

Gas plasma, formed in the discharge region, penetrates in the central source chamber through the slit formed by the top and bottom cathodes (Fig. 2(4)). Negative biased sputtering target is fixed on the water-cooled holder (Fig. 2(6)). Target is set in the central chamber of the source on the line of cathodes slit. Gas ions from the plasma bombard the target and this process leads to the target surface sputtering and heating. Ionization of sputtered atoms follows to the plasma and ionization can be supported also with the secondary electrons knocked out from the acceleration electrode (Fig. 2(8)) if acceleration voltage U_{ac} is applied. This process gives mixed plasma consisting with the gas ions and the ions of the target material.

In the case of "low voltage – high current" operation, with the optimized configuration of the electrodes and magnetic system, plasma, penetrated in the central source chamber, completely envelopes the sputtering target and forms visible plasma boundary near the exit aperture of the source. The plasma boundary position depends on electrodes configuration, plasma operation parameters, sputtering voltage, and applied acceleration voltage. Plasma boundary, in the case, will act as the ions emitter. Under the influence of the acceleration voltage, ions are extracted from the plasma boundary and accelerated towards the holder.

It is noted that the temperature of the sputtering target is an important parameter. Much of the particles sputtered from the target surface have high velocities and the probability of its ionization is rather low, consequently most of them will be deposited on the source and chamber walls. Having high temperature of the target (>1000 °C), the sublimated vapor from the target surface can be obtained,[11] i.e., atoms with the thermal velocities, which have much higher probabilities for the ionization, thus it comes to obtain higher amount of target material ions in the plasma.

It is possible to estimate the maximal equilibrium temperature T_∞, which can be attained on the target, with the simple equation from:[12]

$$T_\infty = \left(\frac{U_t j_t}{2\varepsilon\sigma} + T_0^4\right)^{\frac{1}{4}}, \quad (1)$$

where j_t – ion current density on the target surface, σ – Stefan–Boltzmann constant, and T_0 – initial temperature. Equation takes in the account energy transfer from the bombarding ions U_t and emissivity of the target ε. With the energy of the bombarding ion ~1.5 keV and increasing ion current density from 5 to 15 mA/cm^2, the maximal target temperature can be estimated from about 800 to 1200 °C. Varying cooling water flow through the target holder, additional control of the target temperature shall be done. In the actual process with the plasma current in the discharge region ~1 A and bias on the target – 1.2-1.5 kV, yellow to bright yellow glow of the target is obtained after 3-5 min. operation and is maintained nearly constant during the treatment process.

The target is sputtered during the ion source operation resulting in the mixed gas-metal plasma. In general, dependently on effectiveness of target sputtering, it is possible to vary the metal phase amount in the plasma, thus the operation mode of the source can be varied as: (1) Having zero or minimal target sputtering, the source acts as gas ion source; (2) with the effective target sputtering and proper shape of the target, the source can be applied for the layers deposition with noble or reactive gases; and (3) with the effective ionization of the sputtered material, the source produces mixed gas-metal plasma. The effectiveness of the target sputtering depends on gas pressure, geometry of the electrodes and the target, energy of gas ions, their current density at the target surface, etc. Fig. 4 shows the examples of ion current I_t on titanium target in dependence on the target bias voltage U_t for the different plasma conditions at argon pressure 0.015 Pa. It can be observed that dependence is linear and target current is higher for the higher plasma current. Here, it needs to note that target electrode can be judged as big Langmuir probe. Without bias

voltage the probe has floating potential U_a' which, in the case, is 200-300 V and generally there should be no ion current to the target in the case of $U_t < U_a'$.

For the purpose of the additional plasma focusing and stabilization, the supplemental ring-shape permanent magnet (Fig. 2(7)) was installed on the exit aperture of the ion source.

III. EXPERIMENTAL DETAILS

The purpose of the work was to evaluate how is the influence of the ion source design and operation parameters on the target sputtering process. Series of deposition and implantation experiments were carried on with controlling of the surface layer modification, composition of deposited layers, coating thickness, and substrate sputtering depth measurements. Thickness of the deposited layers was measured as value of target sputtering effectiveness.

Experiments were conducted with the acceleration voltages from 0 to 20 kV. Titanium, carbon, and TiB_2 targets were used for the target sputtering and implantation experiments. For the experiments, ultra pure 6N argon and nitrogen gases were utilized. Gas pressure in the process was computer controlled with the precise gas leak valve. Typical ion current on the holder during the implantation processes was up to 100 μA/cm^2. Implantation fluences for the processes were calculated, considering that only singly charged ions are present in the beam, from the current on the holder and irradiation time with the equation:

$$\Phi = M\frac{J \cdot t}{S}, \tag{2}$$

where Φ – irradiation fluence, ions/cm^2; M - ion flow during one minute ($M = 3.7 \times 10^{17}$ ions/(mA$\times$min)); J - ion current, mA; t - time of implantation, min; S - square of implantation, cm^2. Here it needs to note that, in general, holder current consists not only with the current of accelerated ions, but also with the current of secondary electrons knocked from the holder. Such effect was not considered in the study and actual implantation fluences can be smaller than the calculated ones.

Test pieces of A5052 aluminum alloy (Mg $\sim$ 2.5%, Fe – 0.4%, Cr – 0.2%, Si – 0.25%) with the dimensions 10$\times$10 $\times$5 mm were used for layers deposition experiments and its composition evaluations. WC-9%Co hard alloy test pieces 10$\times$10$\times$5 mm were used in the experiments for evaluation of sputtering depth during the implantation experiments. For the implantation experiments 99.99% pure α-Fe test pieces were used. One face of all the test pieces was polished to the mirror quality. To remove the dislocation hardening, prior to the implantation experiments, α-Fe test pieces were vacuum annealed at 500 °C during 6 h.

Atomic force microscope (AFM) SII NANOPICS 1000 was applied for the purpose of coating thickness and depth of substrate sputtering measurements. This was done applying Silicon glue droplet as the masking on the test piece surface prior to the treatment process. After the treatment, the glue droplet was removed and resulting step was measured with the AFM.

Coatings composition evaluation was performed with scanning electron microscope JEOL-5610 equipped with electron probe microanalysis (EPMA) device. In the case of A5052 test pieces, energy dispersive spectroscopy spectrum peaks from the coatings did not interfere with the substrate spectrum, allowing to distinguish clearly the coating chemical composition.

X-ray photoelectron spectroscopy (XPS) was utilized for the surface layer elements analysis before and after ion implantation experiments. Analysis was performed on PHI-5500 multitechnique spectrometer equipped with spherical capacitor analyzer (SCA) 10-360 model. X-ray source with Al anodes was equipped with monochromator. Area of analysis was $\sim$0.4$\times$0.4 mm around the center of test piece. In order to perform profile analysis, the test pieces' surface was sputtered with argon of 4N purity with incident ion energy 2.5 keV. The XPS setup is equipped with the oil-free evacuation system. Base pressure in analyzer chamber was 2×10^{-7} Pa. Pressure during sputtering was maintained at 5-6$\times10^{-6}$ Pa. Atomic concentrations of elements were estimated from the survey spectra taking into account the area of lines.

Hardness profiles at shallow depths were obtained with SHIMADZU DUH-211 Dynamic Ultra Micro Hardness Tester with using the Oliver and Pharr method[13] with a Vickers indenter. Indentation tests were made with the applied loads ranged from 3 to 500 mN.

IV. RESULTS AND DISCUSSION

A. Effectiveness of target sputtering

Target sputtering experiments were performed for titanium, carbon, and TiB_2 targets. The selection of target materials was determined by its importance for the actual applications. In the tasks of thin films deposition or ion implantation, titanium and carbon are typical elements for the wear and corrosion resistance properties improvement. TiB_2, as it was demonstrated before,[8,10] is the promising target material for the ion implantation tasks for the improvement of materials tribological properties. Shape of the targets was conical with base diameter $\sim$30 mm and angle 112°. U_{ac} in the sputtering processes was set to 0 kV to avoid the influence of substrate surface sputtering. Deposition process duration was typically 60 or 120 min. In Fig. 5, the speeds of layers deposition measured with AFM are presented with the U_t from 0 to -1.5 kV with using argon and nitrogen as working gases. Distance from the source exit aperture to the holder was 30 cm. It can be noted from Fig. 5 that in the case of Ar gas sputtering effectiveness or sputtering yield for the Ti target is about twice higher than that of C and TiB_2 target. For the case of Ti target bombardment with nitrogen (Fig. 5 – "open squares" line) sputtering efficiency is 3 times lower comparing to the case of argon sputtering, which is due to smaller kinetic energies of nitrogen ions and also due to the influence of its chemical reactivity.

With the increase of U_t as well as with the ion energy increasing, the target temperature will rise up to the high levels ($T > 1000$ °C at $U_t > 1$ kV). In general, the process of collisional sputtering should not depend on temperature, if the surface binding energy is constant.[14] But, at the elevated temperatures, due to the reducing of binding energies

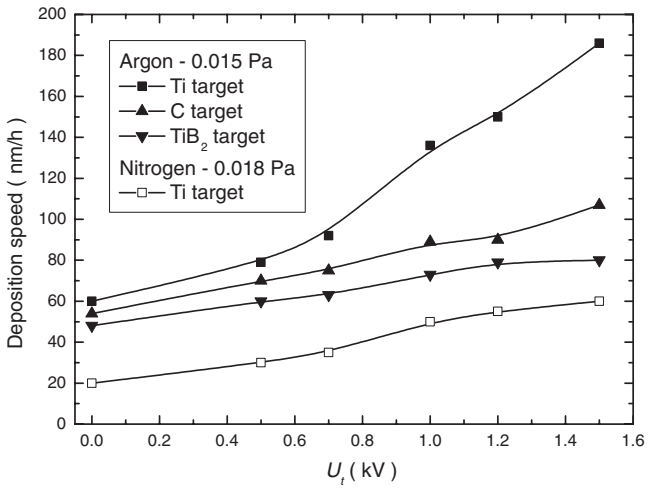

FIG. 5. Coating deposition speed as a function of target bias voltage U_t for titanium, carbon, and TiB_2 targets for the case of $I_{plasma} \sim 1$ A and $U_{ac} = 0$ kV for argon and nitrogen gases.

or heat spike sputtering mechanism activation, the sputtering yield can be increased, however this process may vary significantly for the different materials. Recently temperature influence on the sputtering process was investigated by several authors, mainly for the applications to the magnetron sputtered targets. For example, Zr and Y target shows sputtering yield increasing at the elevated temperatures.[15] Increasing of graphite sputtering yields was observed for the temperatures above 800 °C (Ref. 16) for the case of Ar bombardment. From the other hand, in Ref. 17 it was shown that sputtering yield of Ag can be reduced in the case of elevated temperatures sputtering, but in Ref. 18, the measured sputtering yields of Cu and Ag showed no detectable temperature dependence. In the case of reactive sputtering, the situation can be more complicated due to the diffusion effect, possible phase transformation and formation of additional chemical compounds which can change sputtering yield in one or another way. For an example in Ref. 19, magnetron sputtering of Ti targets at the elevated temperatures was investigated and it was demonstrated that α-Ti–β-Ti transformation at T > 900 °C led to significant reducing of nitrogen and oxygen diffusion coefficients, thus increasing the sputtering efficiency, allowing high sputtering yield to be obtained for the reactive sputtering. In general, it can be said that influence of the elevated temperatures on the sputtering process is connected both with the surface properties modification and with the experiment conditions, also for the different materials distinct mechanisms may be responsible for sputtering yield modification.

In our case, for the sputtering with Ar or N_2 (Fig. 5), gradual increasing of coating deposition speed can be observed for all tested target materials with the increasing of U_t. Lower binding energy and saturated vapor appearance may be effective for the higher deposition rate in the case of Ti target. For C and TiB_2 targets, sputtering efficiency is about same and also lower than that of Ti target, due to the higher binding energies. Obtained temperatures for the C and TiB_2 targets might not be sufficient to create noticeable saturated vapor appearance.

For the experiments, it is difficult to clearly distinguish the influence of the target temperature on the sputtering efficiency from the influence of the ions energy and current. Evidently ions with higher energy and current provide more efficient sputtering, as well as higher target temperature. It was observed as well that the target current I_t increased with the target temperature increasing, which can be due to the enhanced electron emission (thermal or secondary), and maintain nearly constant while target temperature is high. Experiments with the forced target cooling/heating and fixed target ion currents are required for the investigations of temperature influence on the sputtering efficiency.

It needs to note that in the case of deposition with $U_{ac} = 0$ kV, resulting coatings look homogeneous, but rather soft, with low density and exhibit weak adhesion to the substrate. Applying small acceleration voltage $U_{ac} < 1$ kV, ion beam assisting regime of deposition can be achieved, resulting in more dense and solid coating structure with much better adhesion to the substrate.

EPMA analysis of coatings, deposited with the parameters presented on Fig. 5, revealed that the deposited layers consist of target material and reactive gas (if one was used in the process) as expected. Due to the small thickness of the deposited layers, it was not possible to determine well the elements' amount. However, it was detected that, in the case of effective target sputtering, some amount of sputtered material from the discharge chamber walls and discharge cathodes can reach the holder surface, as well as the material from the sputtering target. For an example, in the case of Ti target sputtering, at $U_t = 1.5$ kV, Fe content in the deposited layer was about 1/5 of total Ti content. It was determined that the shape of the discharge cathodes (Fig. 2) influences on the Fe contaminations amount significantly. The surfaces of the cathodes in the slit area are sputtered during the source operation due to the ions bombardment. In the case of parallel cathodes surfaces in the discharge slit, significant flux of the cathodes/walls material to the holder was found. Shape modification of the cathodes slit area with 30° angle between cathodes surfaces allows to reduce Fe flux to the holder surface in about 3-4 times.

Slit size between the top and bottom discharge cathodes (Fig. 2) is an important parameter for the ion gun operation and target sputtering efficiency. If the slit size exceeds several Debye lengths, the plasma from the external discharge chamber can penetrate into the central chamber. Also when slit size exceeds some critical value, the discharge burning stability is reduced. With increasing of the slit size, the target ion current I_t, is increasing, but, in spite of this fact, the maximal efficiency of target sputtering and stable discharge burning was observed at the slit sizes 5 mm < l < 7 mm with the maximum in the range about 6 – 6.5 mm. This is connected with the plasma redistribution inside the central source chamber with the increased slit size and the ion current I_t can be increased due to the increased area of plasma burning in the central chamber, but this growth will not influence on the target sputtering process.

As well as slit size, the target shape also gives influence on the resulting coating deposition or implantation process. Sputtered particles from the target are moving along the lin-

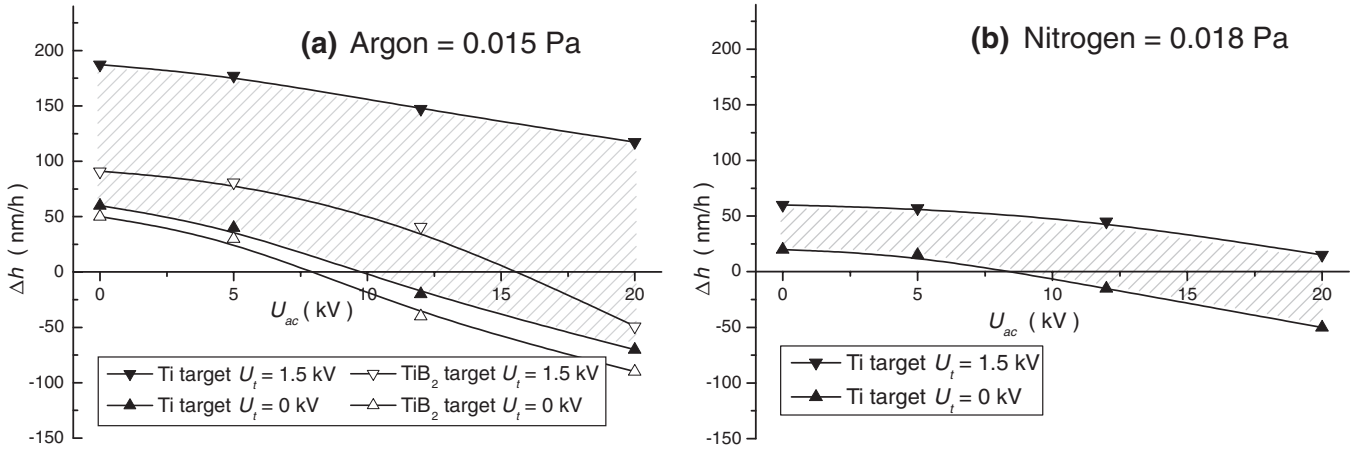

FIG. 6. Variation of surface level of WC-Co test pieces during mixed ion beam treatment with using Ti or TiB_2 sputtering target at the acceleration voltages from 0 to 20 kV, (a) – with using argon as working gas, (b) – with using nitrogen. Zero level of Y axis corresponds to the initial surface level position, $+\Delta h$ – coating deposition, $-\Delta h$ – surface sputtering. Hatched area indicates range of treatment effects for the processes with Ti target with $0\,\text{kV} \le U_t \le 1.5\,\text{kV}$.

ear trajectories, and, resulting thickness distribution of the deposited material on the holder is determined with the geometry of the target and source exit aperture. Having cylindrical target, the most of sputtered material will be deposited on the walls of the source central chamber and, in the case of high temperature target, mainly ionized sublimated vapor from target can reach samples holder. With the target of cone shape and adjusting the cone angle, it is possible to obtain nearly uniform thickness distribution on the effective treatment area, which in our case was about 16 – 17 cm in diameter on the distance 30 cm from the source exit aperture.

With the installation of magnet (Fig. 2(7)), target sputtering effectiveness can be increased about 20% due to the additional plasma magnetization and focusing around the target area, which leads to increasing of the resulting ion current I_t, but also can lead to the non-uniform coating thickness distribution on the treatment area.

Applying voltage U_{ac} to the acceleration electrode, bombardment of the samples holder with the energetic ions from the multi-component plasma is obtained. Dependently on the ion energy, it is possible to obtain the regimes of ion beam sputtering, mixing or implantation. During the operation, there will be two simultaneous (competitive) processes: one is the bombardment of holder with energetic ions from the plasma, and, the other is the deposition of sputtered material from the target. Fig. 6 shows the test pieces surface level variation as a function of U_{ac} for the $U_t = 0$ kV and 1.5 kV, with using argon or nitrogen as working gas. Cone shape with 112° angle Ti target was used in the experiments. Also, for an example, the case for same shape TiB_2 target is presented for Ar treatment processes.

With the increasing of U_{ac}, the competitive process of deposition/sputtering (implantation) will occur. It can be observed that, when sputtering rate is high ($U_t = 1.5$ kV), deposition process is dominant up to high U_{ac} values, but with the decreasing of U_t value, the sputtering process becomes significant. Hatched areas on Fig. 6 indicate range of treatment influences on the surface level deviation Δh for the processes with $0\,\text{kV} \le U_t \le 1.5\,\text{kV}$. According to the data in Fig. 6, appropriate process parameters can be selected. Also, with the adjusting of U_t value, according to the target sputtering effectiveness data from Fig. 5, it is possible to keep Δh close to zero if required.

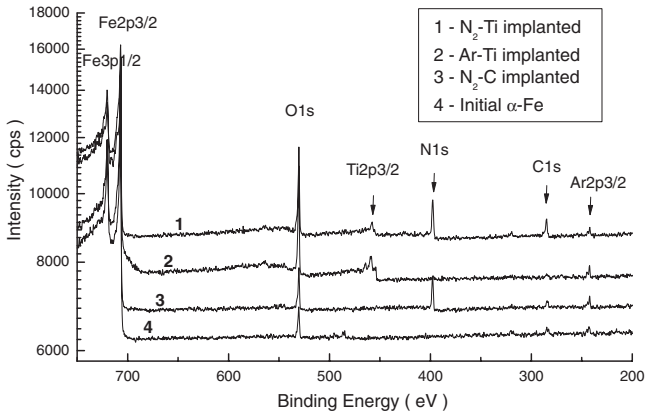

FIG. 7. XPS spectra obtained for α-Fe test pieces after Ar sputtering to the depth ~10 nm. (1) – N_2-Ti ion implanted, (2) – Ar-Ti ion implanted, (3) – N_2-C ion implanted. (4) – non-treated initial condition.

B. Implantation experiments

Mixed ion beam implantation experiments were carried out with the described setup in accordance with the above explanations. In Table I, process parameters, applied for the α-Fe test pieces, are presented. Maximal possible acceleration voltage U_{ac} with the existing installation was 20 kV. Estimation of the penetration depth for ions with the energy 20 keV

TABLE I. Ion implantation process parameters for α-Fe test pieces.

Working gas/ target material	Plasma current, I_{plasma}, A	Target bias, U_t, kV	Acc. voltage, U_{ac}, kV	Fluence, ions/cm^2
N_2-Ti	0.8	500	20	$\sim 3.5\times10^{17}$
N_2-C	0.8	500	20	$\sim 4.3\times10^{17}$
Ar-Ti	1.0	700	20	$\sim 3.6\times10^{17}$

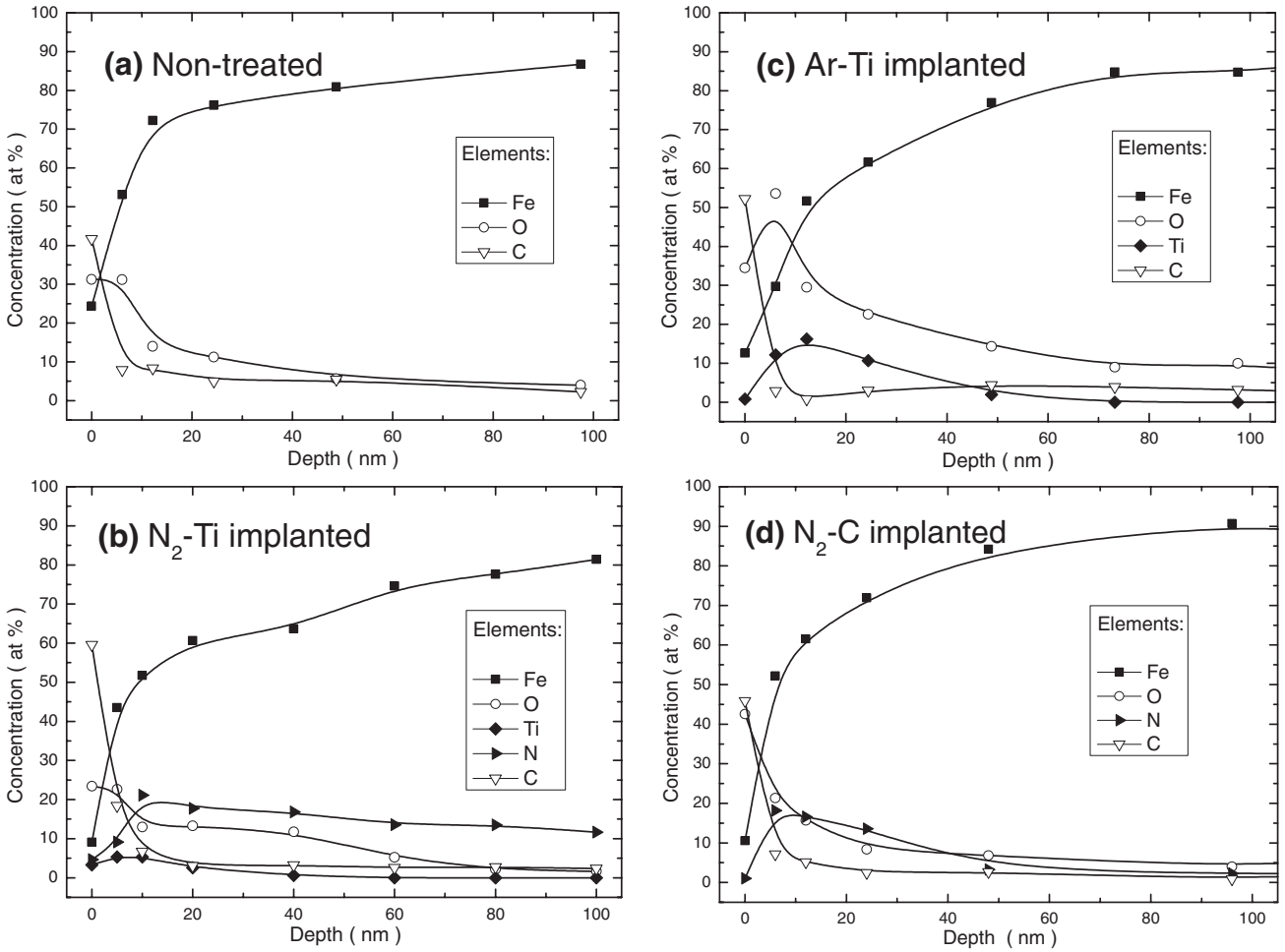

FIG. 8. Surface layer elements depth profiles obtained with the XPS analysis data for the α-Fe test pieces for (a) – not treated initial condition, (b) – N_2-Ti ion implanted, (c) – Ar-Ti ion implanted, (d) – N_2-C ion implanted.

calculated with SRIM2008 code[20] is in the range of 25 nm for nitrogen, and ~9 nm for titanium. With such process parameters, slight surface sputtering can be expected according to Fig. 6.

Examples of XPS analysis spectra taken at the depth about 10 nm for the initial and ion implanted α-Fe test pieces are presented in Fig. 7 and the associated elements concentration depth profiles obtained with using Ar sputtering are presented in Fig. 8.

Appearance of nitrogen and titanium associated peaks can be observed for the relevant processes; also oxygen associated peak is rather high for all the examined test pieces. Maximal obtained nitrogen concentration in the surface layer is about 20 at. %. For the process of Ar-Ti implantation obtained Ti concentration is about 15 at. %. For the 20 keV ions, sputtering yield is rather high, so, with such implantation energies, it seems to be difficult to get higher concentration of implanted elements, due to the simultaneous surface sputtering effect. Measured penetration depths of the implanted elements are in good agreement with the calculated estimations.

The oxygen appearance in the surface layer of the implanted test pieces can be as from the residual gas in the vacuum chamber, as adhered to the chamber and source walls or due to some leakage during the operation. It is obvious that good cleaning and proper maintenance are required to avoid excessive oxygen presence.

In Fig. 9, measured nanoindentaion hardness data as a function of indenter penetration depth for the initial and ion

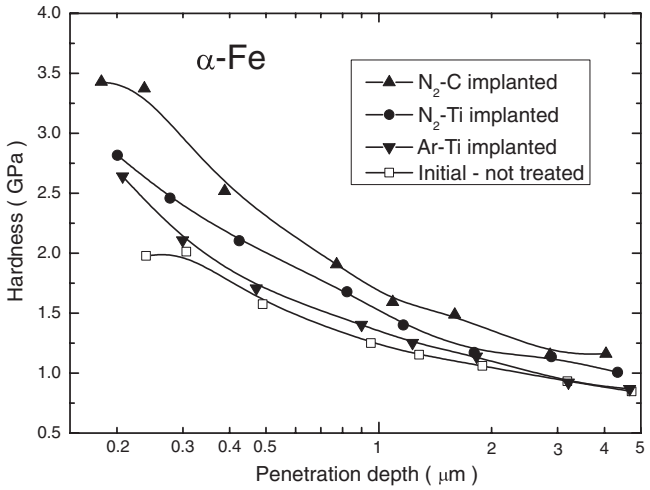

FIG. 9. Dynamic nanohardness as a function of indenter penetration depth for the initial and mixed beam ion implanted α-Fe test pieces.

implanted α-Fe test pieces are presented according to Table I implantation processes.

For all the performed treatments, increasing of surface layer hardness can be observed, with maximal obtained hardness about 3.5 GPa for the N_2-C implantation process. The hardness increase and the difference between the processes can be explained by the formation of chemical compounds in the surface layer due to the multi-component implantation. The smallest hardness growth is observed for the case of Ar-Ti implantation where only dislocation or stress induced hardening can occur.

Precipitates of Ti-N and Fe-C-N are possible at relevant implantation processes leading to the precipitation induced hardening additionally to dislocation mechanism. It needs to note also that the hardening effect can be observed at the depths order of magnitude deeper than actual projected range of the implanted elements. Such phenomenon is usually called as "long-range" implantation effect[21] and is typically explained with the stress-induced dislocation structure formation during the implantation and this effect is especially pronounced for the pure materials.[22]

V. CONCLUSIONS

In-depth investigation of operation parameters, regimes, and configuration was performed for the constructed sputter enhanced ion-plasma source in terms of effectiveness of target sputtering with low pressure discharge plasma. The source has relatively simple design, is inexpensive, and can be utilized both for research tasks and for industrial operation for the purposes of materials surface treatment.

It was demonstrated that varying plasma parameters and target bias voltage, the source can be operated in regimes of layers deposition, ion beam mixing and ions implantation. For the implantation process, it is possible to keep treated surface height deviation with adjusting the target sputtering effectiveness.

Contamination of the resulting multi-component plasma with iron and oxygen was detected, resulting in additional Fe and O content in the implanted layers. Optimization of electrodes shape allows Fe contamination to be reduced to the minimal level. To reduce oxygen content, proper cleaning and maintenance is required.

Multi-component beam experiments with α-Fe test pieces demonstrate possibility to apply the universal ion source for the tasks of ion implantation. Implanted elements depth distributions for 20 keV implantation obtained with XPS depth profiling were found to be in good agreement with the numerical estimation. Mixed beam implantation leads to α-Fe surface hardening from 2 GPa in initial condition up to 3.5 GPa for the N_2-C implanted condition.

[1] J.-P. Hirvonen, F. Harskamp, P. Torri, H. Willers, A. Fusari, N. Gibson, and J. Haupt, Nucl. Instrum. Methods B **127/128**, 922 (1997).
[2] V. P. Sergeev, A. R. Sungatulin, O. V. Sergeev, and G. V. Pushkareva, Proc. TPU **309**, 120 (2006) (UDC 539.12.04:669.14.255:691.793).
[3] W. Ensinger, Rev. Sci. Instrum. **63**, 5217 (1992).
[4] J. K. Hirvonen, Mater. Sci. Rep. **6**, 215 (1991).
[5] Y. Pauleau and P. B. Barna, *Protective Coatings and Thin Films: Synthesis, Characterization, and Applications*, NATO ASI, **21** (Springer, 1997).
[6] J. C. Szcancoski, C. E. Foerster, F. C. Serbena, T. Fitz, U. Kreißig, E. Richter, W. Möller, C. M. Lepienski, P. C. Soares Jr., and C. J. de M. Siqueira, Surf. Coat. Technol. **201**, 1488 (2006).
[7] G. V. Potemkin and V. F. Kalmykov, Instrum. Exp. Tech. **44**, 704 (2001).
[8] V. V. Brukhov, *Tools Durability Increasing by Means of Ions Implantation* (NTL, Tomsk, 2003).
[9] G. V. Potemkin, Russ. J. Non-Ferrous Met. **52**, 103 (2011).
[10] K. V. Shalnov, V. K. Kukhta, K. Uemura, and Y. Ito, Surf. Coat. Technol. **206**, 849 (2011).
[11] L. I. Maissel and R. Glang, *Handbook of Thin Film Technology* (McGraw-Hill, Michigan, 1970).
[12] H. Ryssel and I. Ruge, *Ion Implantation* (John Wiley & Sons Inc, 1986).
[13] W. C. Oliver and G. M. Pharr, J. Mater. Res. **7**, 1564 (1992).
[14] R. Behrisch and W. Eckstein, *Sputtering by Particle Bombardment* (Springer, 2007).
[15] M. Laurikaitis, J. Cyvienė, and J. Dudonis, Vacuum **78**, 395 (2005).
[16] V. Philipps, K. Flaskamp, and E. Vietzke, J. Nucl. Mater. **111/112**, 781 (1982).
[17] H. Y. Lee and H. Y. Chang, Philos. Mag. B **67**, 97 (1993).
[18] J. Bohdansky, H. Lindner, E. Hechtl, A. P. Martinelli, and J. Roth, Nucl. Instrum. Methods B **18**, 509 (1986).
[19] D. Mercs, F. Perry, and A. Billard, Surf. Coat. Technol. **201**, 2276 (2006).
[20] J. F. Ziegler, M. D. Ziegler, and J. P. Biersack, Nucl. Instrum. Methods B **268**, 1818 (2010).
[21] Yu. P Sharkeev and E. V Kozlov, Surf. Coat. Technol. **158/159**, 219 (2002).
[22] A. N. Didenko, E. V. Kozlov, Yu. P. Sharkeev, A. S. Tailashev, A. I. Rjabchikov, L. Pranjavichus, and L. Augulis, Surf. Coat. Technol. **56**, 97 (1993).